Synthesis and Electrical Properties of Well-Ordered Layered α-MoO₃ Nanosheets

R. Naouel[1], H. Dhaouadi[2,*], F. Touati[1,2], N. Gharbi[1]

Abstract: $\alpha-MoO_3$ ordered nanosheets have been synthesized under hydrothermal conditions using commercial MoO_3 and hydroquinone as structuring agent. X-ray diffraction (XRD), scanning electron microscope (SEM) and transmission electron microscopy (TEM) were used to analyse the obtained material. The conductivity mechanism of the Molybdenum ordered nanosheets has been investigated using combined complex impedance and modulus formalism.

The temperature dependence of the conductivity, which was between 473 and 573 K, is very close to the Arrhenius' law, with an activation energy of 0.76 eV. However, the conductivity of the material increases with temperature. It shows a typical negative temperature coefficient resistance (NTCR) similar to that of a semiconductor. The dielectric properties of the MoO_3 compound have been studied in the temperature range of 473-573 K as well as the frequency range of 10 Hz to 13 MHz. The ac-conductivity for high frequency $\sigma_{ac}(\omega)$ obeys the universal power law.

Keywords: Electron microscopy; Hydrothermal synthesis; X-ray diffraction; Electrical properties

Introduction

The control of the morphology and size of nanomaterials has become a dominant theme of study in the material physics field since these parameters are the key elements that determine the physical properties of nanomaterials. Low dimensional nanostructures, such as nanowires, nanorods, nanotubes, nanobelts, and nanosheets are increasingly being given more attention due to their novel electrical, magnetic and optical properties [1-8]. Nanosheet materials have been synthesized using various methods: the vapor-liquid-solid (VLS) process [9], chemical vapor deposition (CVD [10], the solution based method [11] and the Langmuir-Blodgett (LB) technique [12].

It must be noted that the layered transition ox-ides have been given considerable attention in different applications such as in the electrosynthesis of electrochromic molybdenum oxide [13], in gas sensing [14], in catalysis [15], the pillaring method [16] and inactive electrode materials [17]. Among the layered transition metal oxides, orthorhombic MoO_3 has been receiving considerable attention within the field of solid state materials chemistry owing to its fascinating properties and its great potential to be used in many fields such as: in ammonia sensing [18], in alkane dehydrogenation catalysts [19], in supercapacitors [20] and in active anode materials for batteries [21].

In this paper we study, on the one hand, the synthesis and the characterization of the molybdenum oxide nanosheets; and on the other hand, the electrical properties of this nanomaterial. The details concern-

[1]Laboratoire de Chimie de la Matière Condensée, Université de Tunis., Institut Préparatoire aux Etudes d'Ingénieur de Tunis, 2 rue Jawaher Lel Nehru 1089 Montfleury-Tunis (Tunisia)
[2] "Laboratoire des Matériaux Utiles" Institut National de Recherche et d'Analyse Physico-chimique, Pôle technologique de Sidi-Thabet, 2020, Tunis, Tunisie.
*Corresponding author. E-mail: dhaouadihassouna@yahoo.fr

ing the dielectric response of α-MoO₃ as a function of frequency and temperature has been investigated. Due to its layered structure being favorable to lithium insertion, α-MoO₃ nanomaterial appears promising for lithium battery applications.

Methods

Sample preparation

The synthesis was carried out using the hydrothermal process. Sigma-Aldrich molybdenum trioxide (1313-27-5) (0.262 g) and hydroquinone (HDQ) HO-C₆H₄-OH (0.2 g) were introduced in 10 ml of distilled water. The molar ratio of these three components is (1:1:300). This mixture was treated in a Parr bomb at 180°C. The reaction time is 96 h. The cooling time of this system was fixed at 24 h. The pH of the reaction mixture was kept at 7. The resulting black powder was washed with ethanol in order to remove the residual hydroquinone, and then dried at 80°C for 8 h.

Characterization techniques

X-ray diffraction patterns were recorded for all samples using the Panalytical "X'Pert Pro" diffractometer, using Cu K$_\alpha$ radiation (λ=1.54056 Å). The texture of the prepared sample was examined using a Scanning Electron Microscope (SEM) Quanta 200. Transmission electron microscopy (TEM) results were recorded on a JEOL 100 CX II electron microscope operated at 200 kV.

A polycrystalline sample of α-MoO₃ was crushed and pressed at room temperature into a tablet of 13.06 mm in diameter and 1.01 mm in thickness. Dense pellets suitable for electro-physical measurements were heated at 100°C for 24 h. Metallic silver was deposited on both sides and served as electrodes. The pellet was placed between two blocking electrodes in a tubular furnace and subjected to a temperature regulator. Conductivity measurements were carried out from 473 K to 573 K in 5∼20°C intervals by checking the complex impedance spectroscopy with a Hewlett Packard 4129A impedance analyzer. The signal frequency ranged from 10 Hz to 13 MHz.

Results and discussion

Powder X-ray diffraction

The XRD pattern of the resulting product (Fig. 1(b)) differs from that measured on the commercial molybdenum oxide precursor (Fig. 1(a)). This means that the structure of the obtained material is different from that of the precursor, indicating that the intercalation of HDQ is taking place during the present process. The

obtained material is well defined as a pure phase of MoO₃ that crystallizes in the orthorhombic system with Pnma space group symmetry (JCPDS data, card number 65-2421). The lattice parameters were refined using the WinCELL program with a=3.9728 Å, b=13.8023 Å and c=3.6710Å. It is to be noted that three intense reflections (020), (040) and (060) were observed in the XRD pattern, indicating the formation of a layered structure of MoO₃. Figure 2 shows the projection of the layered structure of molybdenum oxide along the (001) direction.
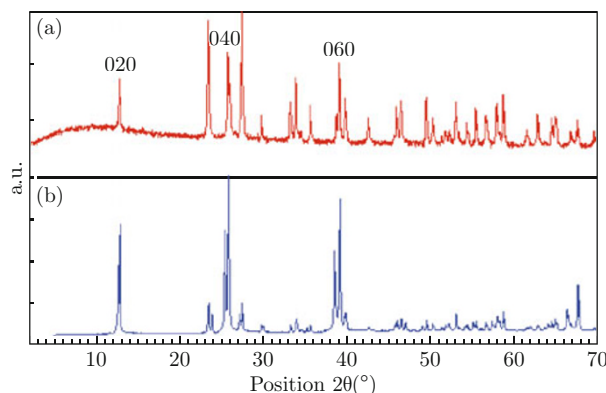

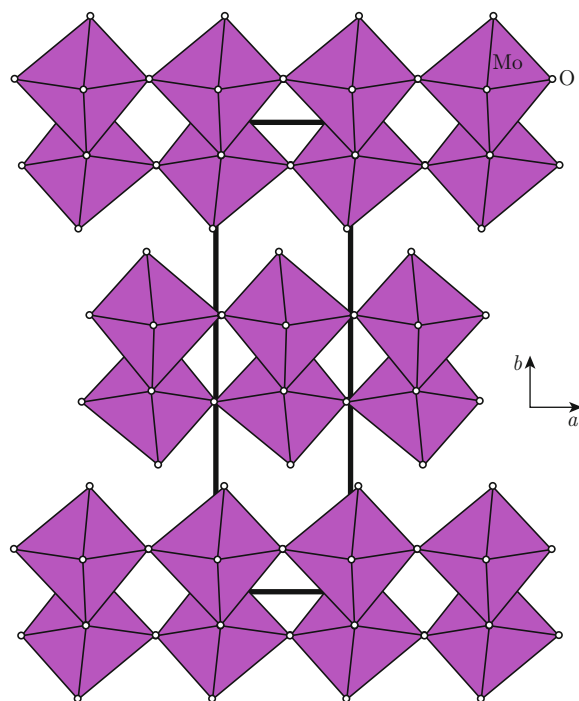Fig. 1   XRD patterns of commercial molybdenum oxide (a) and the obtained product (b).

Fig. 2   Crystal structure for MoO₃ nanosheets.

SEM and TEM

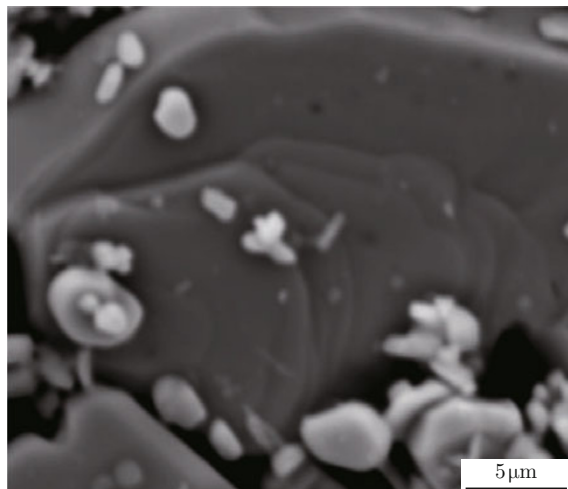The SEM micrograph of the obtained material (Fig. 3) proves the presence of a stratified structure.

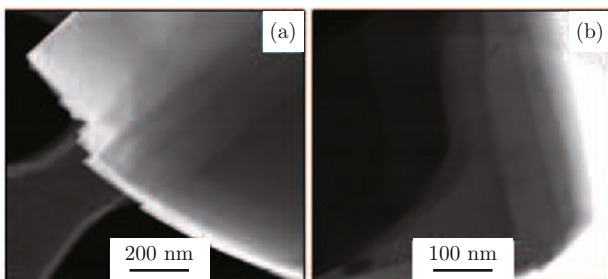Fig. 3   SEM image of the synthesized sample for MoO_3 nanosheets.

Fig. 4   TEM images of the synthesized sample for MoO_3 nanosheets.

This morphology is confirmed by the TEM micrographs which show the presence of well-ordered regular sheets composed of a series of flake sheets. The layered structure can be clearly seen in (Fig. 4(a)) and (Fig. 4(b)). This result is corroborated by the increase of the 0k0 peaks observed in the XRD pattern of the synthesized phase, indicating the well-orientated structure of the material. Yi Jing et al. [22] have synthesized a similar phase by intercalating a long chain of alkylamine in the pre-treated molybdenum trioxide with p-(N-ethyl-N-ethylamino trimethylquaternary ammonium methylsulfate salt)-p'-(nitro)-o'-(chloro) azobenzene (GTL). Taking into account the absence of polarity and the strong electronegativity of the oxygen in the hydroxyl group in the organic precursor used, we can explain the instability of the layer.

Complex impedance analysis

Figure 5 shows the results of the research performed on the electrical properties of MoO_3, using impedance analysis. Figure 5(a) shows the complex impedance spectra (Nyquist plots) at different temperatures for the MoO_3 nanomaterials. The impedance spectrum is characterized by the appearance of a single parabola with a radius that decreases with increasing temperature. The

intercept of the parabola with the real axis (Z') gives us an estimated resistance (R_b) for the material. It has been observed that the resistance decreases with increasing temperature for MoO_3 nanomaterials. The result may be interpreted as a negative temperature coefficient resistance (NTCR) similar to that observed in a semiconductor. The electrical behavior observed in the material may be represented by an equivalent electrical circuit as shown in Fig. 5(a) (Inset).

Figure 5(b) shows the variation of the real part of impedance (Z') as a function of frequency at different temperatures. It has been observed that the impedance value is higher at low temperatures in the low frequency domain; but gradually decreases with increasing temperature. The decrease in Z' with a rise in temperature and frequency indicates a possible increase of the ac-conductivity with the increase in temperature and frequency.

Figure 5(c) represents the variation of the imaginary part of Z'' (impedance loss spectrum) with frequency. It is characterized by the appearance of peaks at a particular frequency in the temperature range [473~573 K]. The appearance of a peak in the loss spectrum is an indication of the beginning of electrical relaxation in the material at different temperatures. The peaks that appear are asymmetric and their positions appear to be shifting towards the higher frequency side with increasing temperature. The variation of the conductivity, calculated from the complex impedance plots, with reciprocal temperature for MoO_3 is shown in Fig. 5(d). The conductivity obeys the Arrhenius' law (σ=Cexp(-E_a/kT), where E_a is the activation energy and k is the Boltzmann constant. The corresponding activation energy E_a=0.76 eV.

Electrical conductivity analysis

Figure 6 shows ac-conductivity $\sigma_{ac}(\omega)$ vs. frequency plots for different temperatures. Inspection of these plots over the measured temperature range reveals the presence of a low frequency conductivity plateau, followed by high frequency conductivity dispersion with a change in gradient. The temperature at which grain resistance dominates over grain boundary resistance is marked by a change in gradient of ac-conductivity with frequency. The frequency at which the change in gradient takes place is known as the critical or hopping frequency. The hopping frequency shifts to higher frequencies with increasing temperature, suggesting a possible enhancement in the carrier-hopping rate of the mobile charge carriers with a rise in temperature. It is seen from Fig. 6 that σ_{ac} increases with increasing frequency and becomes independent of frequency at higher values where the ac electrical conductivity (σ_{ac}) values are very close to each other. These results suggest that the nature and mechanism of the conductivity
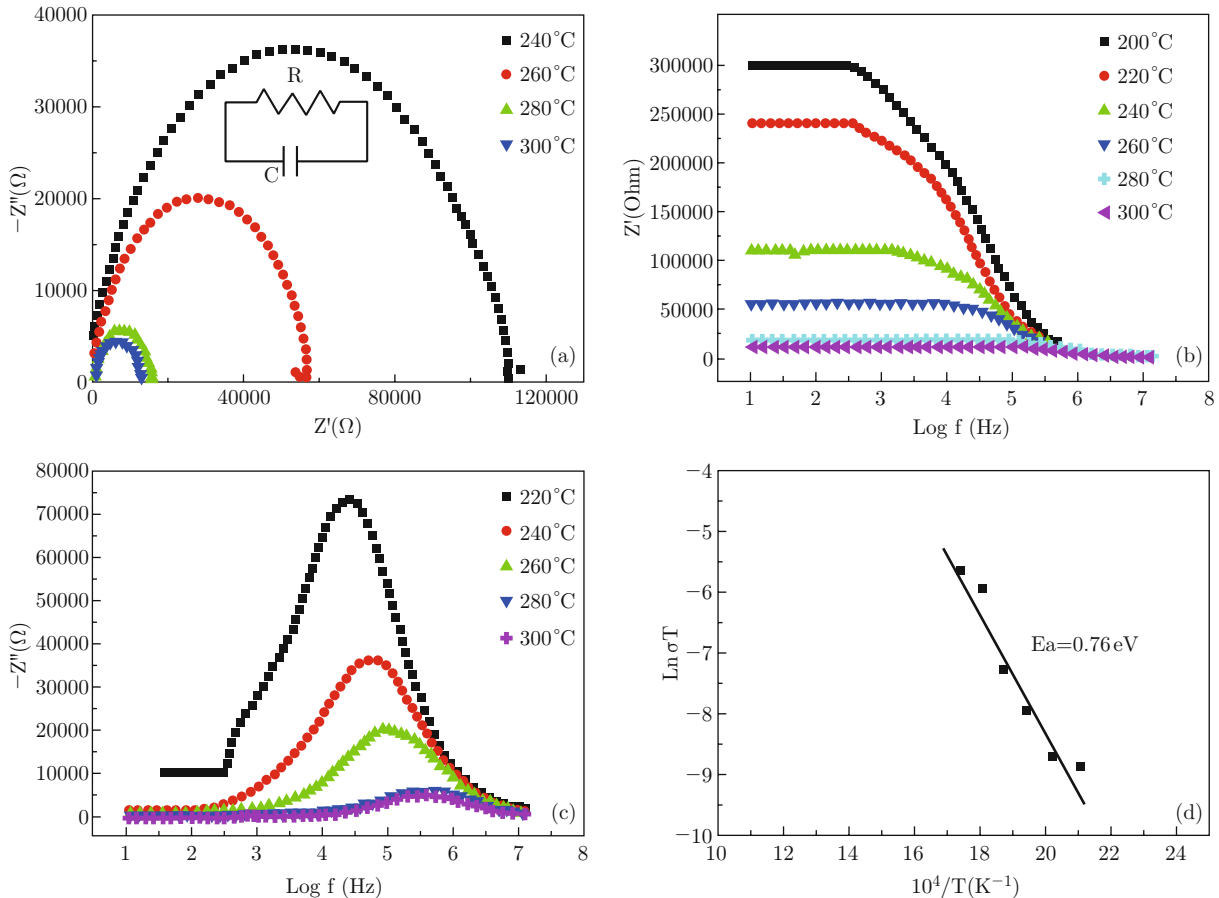
Fig. 5   (a) Nyquist diagrams at different temperatures; (b-c) Z' and $-Z''$ versus frequency at different temperatures; (d) dependence of Ln(σT) on temperature for MoO_3 nanosheets.

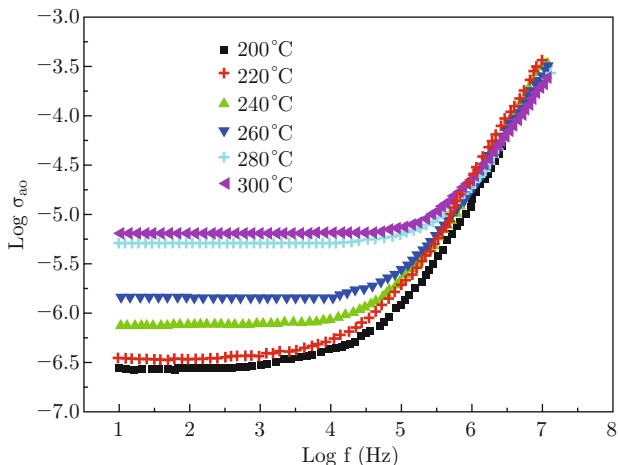Fig. 6   Dependence of Ln(σ_{ac}) on frequency at different temperatures for MoO_3 nanosheets.

dispersion of MoO_3 nanosheets can be analysed using Jonscher's power law defined as: $\sigma_{ac}(\omega) = \sigma_{dc}[1 + (\omega/\omega_H)^n]$ (1) [23-25], where σ_{dc} is the dc-conductivity in a particular range of temperatures, n is the temperature-dependent exponent in the range $0 \leq n \leq 1$ of the interionic coupling strength and ω_H is the hopping frequency at which a change in gradi-

ent of the conductivity occurs. The required σ_{dc} values were obtained from the $\sigma_{ac}(\omega)$ spectrum in equation (1) by using $\sigma_{ac}(\omega_H) = 2\sigma_{dc}(2)$.

Dielectric analysis

Figure 7 shows the variation of the dielectric constant (ε' and ε'') as a function of frequency at selected temperatures (473~573℃) for MoO_3 nanosheets. Figure 7(a) shows that the dielectric constant (ε') decreases at lower frequencies and remains constant at higher frequencies. The constant decrease of the value of the dielectric constant with increasing frequency may be attributed to electronic, ionic and interfacial polarization at low frequencies [26]. Generally, the observed dielectric dispersion at low frequencies can be explained based on the Maxwell-Wagner model of interfacial polarization [27]. According to the Maxwell-Wagner model, the dielectric structure of ferrites consists of two layers: the first layer consists of a large number of grains and acts as a conducting layer at higher frequencies, while the second layer consists of grain boundaries that act as a highly resistive medium at lower frequencies. At low frequencies, the polarization process in MoO_3 nanoparticles can be explained
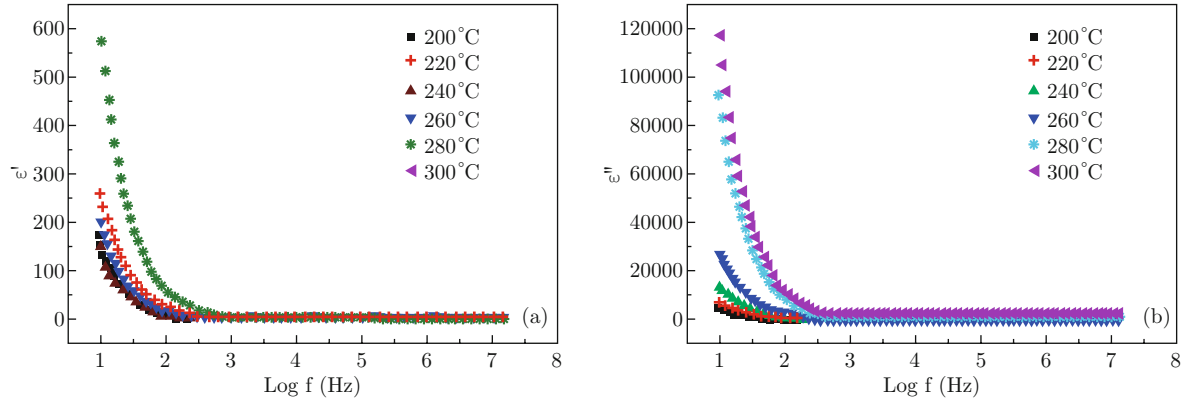
Fig. 7 (a) ε' versus frequency at different temperatures for MoO_3 nanosheets; (b) ε'' versus frequency at different temperatures for MoO_3 nanosheets.
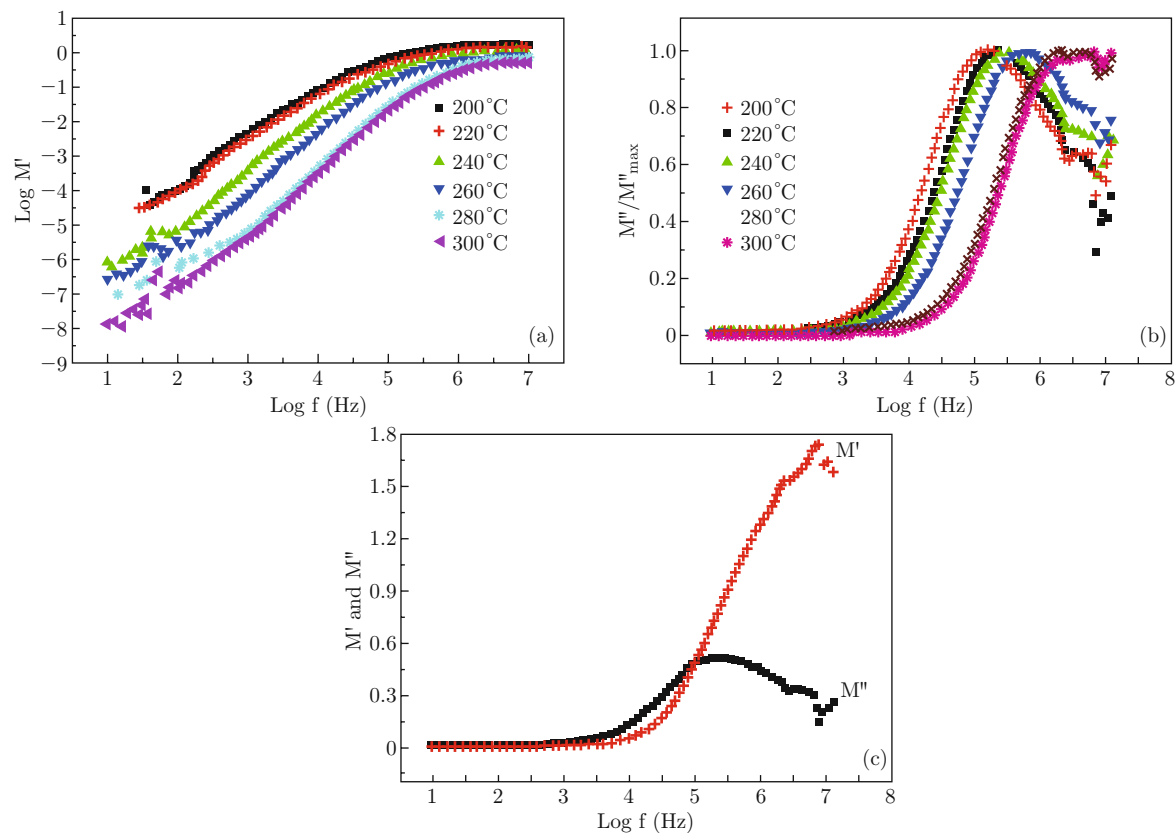

Fig. 8 (a) M′ versus frequency at different temperatures; (b) M″/M″$_{max}$ versus frequency at different temperatures; (c) M′ and M″ versus frequency at 200 °C.

by the dipole orientation in the direction of the applied field. Whereas, at high frequencies, the dipole orientation cannot follow the fast alternating field and therefore its contribution to polarization ceases.

In Fig. 7(b) we can observe that the MoO_3 nanosheets show a decrease in the complex dielectric constant value of ε'' with increasing frequency until reaching a constant value. For nanometer-sized particles, the contribution of the interfacial loss and the loss from electrical conductivity is dominant at lower frequencies, however, at high frequencies, these losses are negligible. This may be the reason for the decrease in the dielectric constant value (ε'') at high frequencies. The large value of the dielectric constant ε'' at lower frequencies is due to the predominance of many species such as oxygen vacancies and grain boundary defects [28].

Modulus formalism

The electrical response of the MoO_3 nanomaterial has also been analyzed via the complex electric modulus

$M^*(\omega)$ formalism [29]. The complex modulus is defined as $M^*=i\omega C_0 Z^*$, where C_0 is the vacuum capacitance of the cell, $\omega=2\pi f$ and $i^2 = -1$. This formalism was adopted because it ignores the electrode polarization and other interfacial effects in solid electrolytes [30-34].

For a given temperature and frequency, the real part (M') and the imaginary part (M'') of the M^* complex modulus ($M^*=M'+jM''$) have been calculated from the complex data ($Z^*=Z'-jZ''$) using the relations $M' = \omega C_0 Z''$ and $M''=\omega C_0 Z'$. A plot of log M' and the normalized M''/M''_{max} imaginary part of the complex modulus versus frequency (in a logarithmic scale) are given in Fig. 8(a) and Fig. 8(b) for the [200~300℃] temperature range. Whatever the temperature, the value of M' reaches a maximum ($M'_\infty=1/\varepsilon_\infty$) at high frequencies. At low frequencies, it decreases sharply and approaches zero, indicating that the electrode polarization phenomena make a negligible contribution to $M^*(\omega)$ and may be ignored when the electric data is analyzed in this way.

In Fig. 8(b), we introduce the (M''/M''_{max}) dependence of log f relative for the MoO_3 nanomaterial at various temperatures. Inspection of these plots over the measured temperature range reveal the presence of a peak which shifts from low to high frequency as the temperature is raised. The modulus peak maxima is defined by $\tau\omega_{max}=1$, where τ is the most probable relaxation time [35-36]. The relaxation process probably originates from the charge carrier hopping mechanism. Observation of the M''/M''_{max} plots shows the absence of any additional peaks at lower frequencies, which indicates a negligible contribution of grain boundary and electrode effects to the total conductivity. In these figures we observe a maximum in the imaginary part, which corresponds to an inflexion in the curve of the real part of Fig. 8(c). This behavior indicates the presence of a relaxation phenomenon.

Conclusion

In this investigation we have developed a simple method for the synthesis of molybdenum trioxide nanosheets, at a relatively low temperature via a hydrothermal process. It has been outlined in this report that this nanostructure is well-ordered and oriented. We suggest that the role of the organic precursor is fundamental in structuring the molybdenum oxide layers. Due to its structure, the electrical conductivity could be the most important bulk property of the molybdenum trioxide. Indeed, the temperature dependence of the conductivity between 473 and 573 K of the MoO_3 nanomaterial indicates that it obeys the Arrhenius' law, with activation energy of 0.76 eV. The frequency dependence of the ac-conductivity is approximated by a universal power law.

References

[1] K. Chung chin, C. K. Poh, G. L. Chong, J. Lin , C. H. Sow and A. T. S. Wee, Appl. Phys. A 90, 623 (2008).

[2] Z. P. Feng, G. R. Li , J. H. Zhong, Z. L. Wang, Y. N. Ou and Y. X. Tong, Electrochem. Commun. 11, 706 (2009). http://dx.doi.org/10.1016/j.elecom.2009.01.001

[3] E. Comini, G. Faglia, G. Sberveglieri, D. Calestani, L. Zanotti, M. Zha.Sensors and Actuators B 111, 2 (2005). http://dx.doi.org/10.1016/j.snb.2005.06.031

[4] Z. L. Wang, Annu. Rev. Phys. Chem. 55, 159 (2004). http://dx.doi.org/10.1146/annurev.physchem.55.091602.094416

[5] J. Wang, G. Dub, R. Zeng, B. Niua, Z. Chen, Z. Guoc and S. Dou, Electrochimica Acta 55, 4805 (2010). http://dx.doi.org/10.1016/j.electacta.2010.03.048

[6] C. Santato, M. Odziemkowski, M. Ulmann and J. Augustynski. J. Am. Chem. Soc. 123, 10639 (2001). http://dx.doi.org/10.1021/ja011315x

[7] K. Pan, Q. Zhang, Q. Wang, Z. Liu, D. Wang, J. Li and Y. Bai, Thin Solid Films 515, 4085 (2007). http://dx.doi.org/10.1016/j.tsf.2006.11.007

[8] B. Yan, L. Liao, Y. You, X. Xu, Z. Zheng, Z. Shen, J. Ma, L. Tong and T. Yu, Adv. Mater. 21, 2436 (2009). http://dx.doi.org/10.1002/adma.200803684

[9] Y. Chen, J. Li, Y. Han, X. Yang and J. Dai, J. Crystal Growth 245, 163 (2002). http://dx.doi.org/10.1016/S0022-0248(02)01690-1

[10] X. S. Fang, C. H. Ye, X. S. Peng, Y. H. Wang, Y. C. Wu and L. D. Zhang, J. Crystal Growth 263, 263 (2004). http://dx.doi.org/10.1016/j.jcrysgro.2003.11.056

[11] B. W. Li, M. Osada, T. C. Ozawa, R. M. K. Akatsuka1, Y. Ebina, H. Funakub, S. Ueda, K. Kobayashi and T. Sasaki, Jap. J. Appl. Phys. 48, 09KA15 (2009).

[12] T. Yamaki, R. Shinohara and K. Asai, Thin Solid Films 393, 154 (2010). http://dx.doi.org/10.1016/S0040-6090(01)01063-X

[13] R. S. Patil, M. D. Uplane and P. S. Patil, Int. J. Electrochem. Sci. 3, 259 (2008).

[14] M. B. Rahmani, S. H. Keshmiri, J. Yu, A. Z. Sadek, L. Al-Mashat, A. Moafi, K.Latham, Y.X. Li, W. Wlodarski and K. Kalantar-zadeh, Sensors and Actuators B 145, 13 (2010). http://dx.doi.org/10.1016/j.snb.2009.11.007

[15] C. Tagusagawa, A. Takagaki, K. Takanabe, K. Ebitani, S. Hayashi and K. Domen, J. Catalysis 270, 206 (2010). http://dx.doi.org/10.1016/j.jcat.2009.12.019

[16] G. Xianji, H. Wenhua,Y. Qijie,C. Yi, Chin. Sci. Bull. 48, 101 (2003). http://dx.doi.org/10.1360/03tb9021

[17] Y. Lu, M. Wei, Z. Wang, D. G. Evans, X. Duan, Y. Lu, M. Wei, Z. Wang, David G. Evans and X. Duan, Electrochem. Commun. 6, 672 (2004). http://dx.doi.org/10.1016/j.elecom.2004.04.023

[18] A. K. Prasad, P. I. Gouma, D. J. Kubinski, J. H. Visser, R. E. Soltis and P. J. Schmitz, Thin Solid Films 436, 46 (2003). http://dx.doi.org/10.1016/S0040-6090(03)00524-8

[19] E. Heracleous, A. F. Lee, I. A. Vasalos and A. A. Lemonidou, Cataly. Lett. 88, 47 (2003). http://dx.doi.org/10.1023/A:1023534816277

[20] T. Brezesinski, J. Wang, S. H. Tolbert and B. Dunn, Nat. Mater. 9, 146 (2010). http://dx.doi.org/10.1038/nmat2612

[21] L. A. Riley, S. H. Lee, L. Gedvilias and A. C. Dillon, J. Power Sources 195, 588 (2010). http://dx.doi.org/10.1016/j.jpowsour.2009.08.013

[22] Y. Jing, Q. Pan, Z. Cheng, X. Dong and Y. Xiang, Mater. Sci. Eng. B 138, 55 (2007). http://dx.doi.org/10.1016/j.mseb.2007.01.015

[23] R. M. Hill and A. K. Jonscher, J. Non-Cryst. Solids 32, 53 (1979). http://dx.doi.org/10.1016/0022-3093(79)90064-4

[24] N. F. Mott and E. A. Davis, "Electronic Processes in Non-Crystalline Materials", Clarendon Press, Oxford, 1979.

[25] R. H. Chen, R. Y. Chang and S. C. Shern, J. Phys. Chem. Solids 63, 2069 (2002). http://dx.doi.org/10.1016/S0022-3697(02)00196-8

[26] A. Kumar, B. P. Singh, R. N. P. Choudhary and A. K. Thakur, Mater. Chem. Phys. 99, 150 (2006). http://dx.doi.org/10.1016/j.matchemphys.2005.09.086

[27] K. W. Wagner, Ann. Phys. 40, 817 (1913). http://dx.doi.org/10.1002/andp.19133450502

[28] J. C. Maxwell, "Electricity and magnetism", Oxford University Press, p 828 (1973)

[29] S. Lanfredi, P. S. Saia, R. Lebullenger and A. C. Hernaldes, Solid State Ionics 146, 329 (2002). http://dx.doi.org/10.1016/S0167-2738(01)01030-X

[30] D. P. Almond, A. R. West and R. Grant, Solid State Commun. 44, 1277 (1982). http://dx.doi.org/10.1016/0038-1098(82)91103-6

[31] B. V. R. Chowdari and K. Radhakrishnan, J. Non-Cryst. Solids 110, 101 (1989). http://dx.doi.org/10.1016/0022-3093(89)90187-7

[32] D. P. Almond, G. Duncan and A. R. West, Solid State Ionics 8, 159 (1983). http://dx.doi.org/10.1016/0167-2738(83)90079-6

[33] B. V. R. Chowdari and K. Radhakrishnan, J. Non-Cryst. Solids 108, 323 (1989). http://dx.doi.org/10.1016/0022-3093(89)90304-9

[34] D. P. Almond and A. R. West, Solid State Ionics 11, 57 (1983). http://dx.doi.org/10.1016/0167-2738(83)90063-2

[35] A. K. Jonscher, "Dielectric Relaxation in Solids", Chelsea Dielectrics Press, London (1983).

[36] J. R. Macdonald, "Impedance Spectroscopy", John Wiley & Sons, New York (1987).